Thin three-dimensional droplets on an oscillating substrate with contact angle hysteresis

J. Bradshaw* and J. Billingham
School of Mathematical Sciences, University of Nottingham, University Park, Nottingham, NG7 2RD, United Kingdom
(Received 6 February 2015; revised manuscript received 11 June 2015; published 19 January 2016)

Recent experiments [P. Brunet, J. Eggers, and R. D. Deegan, Phys. Rev. Lett. **99**, 144501 (2007)] have shown that a liquid droplet on an inclined plane can be made to move uphill by sufficiently strong, vertical oscillations. In order to investigate this counterintuitive phenomenon we use a model in which liquid inertia and viscosity are assumed negligible so that the motion of the droplet is dominated by the applied acceleration due to the oscillation of the plate, gravity, and surface tension. We explain how the leading order motion of the droplet can be separated into a spreading mode and a swaying mode. For a linear contact line law, the maximum rise velocity occurs when these modes are in phase. We show that, both with and without contact angle hysteresis, the droplet can climb uphill and also that, for certain contact line laws, the motion of the droplet can produce footprints similar to experimental results. We show that if the two modes are out of phase when there is no contact angle hysteresis, the inclusion of hysteresis can force them into phase. This in turn increases the rise velocity of the droplet and can, in some cases, cause a sliding droplet to climb.

DOI: 10.1103/PhysRevE.93.013123

I. INTRODUCTION

In Ref. [1], Brunet, Eggers, and Deegan showed that if a fluid droplet is placed on an inclined plane, which is then strongly, sinusoidally oscillated in the vertical direction, the droplet can travel uphill. In a related experiment, Noblin, Kofman, and Celestini [2] placed a droplet on a horizontal surface and applied horizontal and vertical oscillations of different amplitudes and with a phase difference. They discovered that by changing the amplitudes and phase they could change the speed and direction of motion of the droplet. By choosing the phase appropriately, they could directly relate their experiments to those of Brunet *et al.* [1].

The literature on modeling the unsteady motion of contact lines is less extensive than that on steady contact line motion. Papers on experiments and theory for steady moving contact lines, for example Refs. [3–6], suggest that, at least for steady flow, it is reasonable to assume that the contact line velocity is a single-valued function of contact angle. This includes the case of rough surfaces [7], for which contact angle hysteresis may exist, so that for a finite range of contact angles bounded by the static advancing and receding contact angles (θ_A and θ_R), the contact line is pinned. Various authors have used this assumption to model the unsteady motion of contact lines, for example Refs. [8] and [9], although the work of Ting and Perlin [10], and indeed Brunet *et al.* [1], casts some doubt on the validity of this approach since the contact line velocity may not actually be a single valued function of the apparent contact angle. Setting this aside for the moment, in this paper we investigate the effect of various contact line laws on the rise velocity of thin, three-dimensional droplets for which both viscous forces and inertia are negligible. This builds on the work of Benilov [11], who studied this situation when the amplitude of the driving oscillation is small. In this case the droplet can either climb up or slide down the substrate. Benilov also compared the difference between two- and three-dimensional models of the droplet. By using a boundary integral method we are able to solve the three-dimensional problem for arbitrary amplitudes of oscillation. This allows us extend the results of Ref. [11] to larger amplitude oscillations as well as study the effects of alternate contact line laws and hysteresis.

A related model was studied by Benilov and Billingham [12], who used the two-dimensional shallow water equations to examine the effect of inertia, and by John and Thiele [13], who considered the Stokes flow limit. Although our understanding of the possible mechanisms by which the velocity of oscillating droplets is determined has grown, in all of this work, a quantitative comparison with the experiments presented in Ref. [1] has yet to be made.

In this paper, we model the droplet using the quasistatic approximation [14], assuming that the inertial and viscous forces are weak in comparison to surface tension and the acceleration due to gravity and the oscillating plate. This approach allows us to simplify the governing equations and solve for the height of the free surface alone. The benefits of this model are that it is three-dimensional and allows us to include contact angle hysteresis and examine how this causes a change in the droplet's motion as well as attempt to make qualitative comparisons to Ref. [1]. In Sec. II we derive the governing equations and describe our numerical solution method. In Sec. III A we compare our results to the asymptotic solutions for small amplitude oscillations derived by Benilov [11]. In Sec. III B we include contact angle hysteresis, while in Sec. III C we look at an alternative contact line law. Finally, in Sec. III D we study the shape of the footprint of the droplet for both a stationary and an oscillating substrate and the surface of the droplet as the substrate oscillates, and we conclude in Sec. IV.

II. THE MODEL

Consider a droplet of liquid of density ρ, kinematic viscosity ν, and surface tension σ on a plane, solid substrate that is inclined at an angle α to the horizontal and oscillating sinusoidally and vertically. We fix the frame of reference so that the substrate lies in the plane $z = 0$ and the positive x

*pmxjb3@nottingham.ac.uk

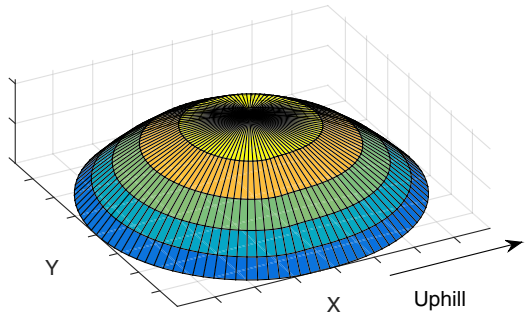

FIG. 1. A droplet and the coordinate system.

axis is uphill. This means that gravity and the acceleration due to the substrate can be combined to make an effective gravity acting at an angle $\pi/2-\alpha$ to the x axis, given by $a(t) = g + a_0 \sin\omega t$, where g is the acceleration due to gravity and a_0 and ω are the acceleration and frequency of the oscillations of the substrate. The domain of solution for this problem is the droplet, $0 \leqslant z \leqslant h(x,y,t)$, where h is the height of the free surface above the plane $z = 0$ and x and y lie in the footprint of the droplet, $\mathcal{R}(t)$. The contact line is at $z = 0$ and $x, y \in \partial\mathcal{R}(t)$ as shown in Fig. 1. By writing the body forces per unit volume as the potential of the effective gravity, we can write the Navier-Stokes equations as

$$\rho\frac{d\mathbf{u}}{dt} = -\nabla p + \rho\nu\nabla^2\mathbf{u} - \rho a\nabla(x\sin\alpha + z\cos\alpha), \quad (1)$$

$$\nabla\cdot\mathbf{u} = 0. \quad (2)$$

The traction boundary condition at the free surface is

$$\mathbf{Sn} = \sigma\kappa\mathbf{n}, \quad \text{on } z = h(x,y,t),$$

where $\mathbf{S}$ is the stress tensor, $\mathbf{n}$ is the outward unit normal, σ is the surface tension, and κ is the curvature of the surface. The stress tensor is $\mathbf{S} = -p\mathbf{I} + 2\rho\nu\mathbf{e}$, where $\mathbf{I}$ is the unit tensor and the components of $\mathbf{e}$ are $e_{ij} = \frac{1}{2}(\frac{\partial u_i}{\partial x_j} + \frac{\partial u_j}{\partial x_i})$. By expressing the curvature as minus the divergence of the normal, the traction boundary condition perpendicular to the surface becomes

$$p - 2\rho\nu\mathbf{n}\cdot(\mathbf{en}) = \sigma\nabla\cdot\mathbf{n}, \quad \text{on } z = h(x,y,t). \quad (3)$$

We also have

$$h(\mathbf{x},t) = 0, \quad \text{for } x,y \in \partial\mathcal{R}(t). \quad (4)$$

A final constraint is the conservation of mass,

$$\rho\iint_{\mathcal{R}(t)} h(x,y,t)\mathrm{d}x\mathrm{d}y = M, \quad (5)$$

where M is the initial mass of the droplet. We will assume that the velocity of the contact line is a function of the contact angle,

$$\mathbf{n}\cdot\frac{d\mathbf{x}}{dt} = v(\theta), \quad \text{for } x,y \in \partial\mathcal{R}(t), \quad (6)$$

where the normal along the contact line points away from the droplet and $v(\theta)$ is a known function, which is positive for $\theta > \theta_A$, negative for $\theta < \theta_R$, and zero for $\theta_R \leqslant \theta \leqslant \theta_A$, where θ_A and θ_R are the advancing and receding contact angles. When the model includes hysteresis these angles are different with $\theta_A > \theta_R$, but when it does not they both equal the equilibrium contact angle $\theta_A = \theta_R \equiv \theta_0$. In Benilov's small amplitude forcing solutions, [11], the forcing from the substrate is small enough to cause only a small change from the equilibrium contact angle, in which case the contact line velocity can be written as a Taylor expansion about θ_0,

$$v(\theta) = V'(\theta-\theta_0) + \tfrac{1}{2}V''(\theta-\theta_0)^2 + \cdots, \quad (7)$$

where V', V'' are the first and second derivatives of the contact line law at equilibrium. In order to simplify Eqs. (1)–(7) we will write the equations in dimensionless form, using scaled variables [11],

$$x = R_0\hat{x}, \quad y = R_0\hat{y}, \quad z = R_0\theta_0\hat{z}, \quad u = U\hat{u}, \quad v = U\hat{v},$$
$$w = U\theta_0\hat{w}, \quad \theta = \theta_0\hat{\theta}, \quad a = a_0\hat{a}, \quad t = T\hat{t},$$
$$p = \frac{\sigma\theta_0}{R_0}\hat{p}, \quad \omega = \frac{1}{T}\hat{\omega}.$$

Here a_0 is the maximum acceleration of the oscillating plate, $U = R_0/T$ and $T = \sqrt{R_0/g}$. We have scaled the pressure using the capillary pressure scale and also, in order to make it easier compare our solution to Benilov's, we define R_0 such that $2\pi\rho\theta_0 R_0^3 = M$. Applying these scalings and rearranging gives rise to the dimensionless parameters,

$$\epsilon = \frac{\rho a_0 R_0^2\sin\alpha}{\sigma\theta_0}, \quad \gamma = \frac{\theta_0}{\tan\alpha},$$

which characterize the strength of the effective gravitational force relative to surface tension and the ratio of the slope of the droplet's surface to the slope of the substrate. The other dimensionless parameters are

$$\delta_1 = \frac{\rho R_0^2 g}{\sigma\theta_0}, \quad \delta_2 = \frac{\rho\nu\sqrt{R_0 g}}{\sigma\theta_0^3},$$

and represent the balance between the inertial and viscous forces and the droplet's surface tension, respectively. Our approach will be to simplify Eqs. (1)–(7) by taking only the leading order terms when $\delta_1, \delta_2, \theta_0 \ll 1$. In order to evaluate how accurate these assumptions are we will use typical values of each parameter from Ref. [1] (see Table I) to estimate the sizes of the dimensionless parameters. To make some progress, we have assumed that $\theta_0 \ll 1$ so that we can use the small slope approximation. Although this Table I shows that θ_0 is not small in the experiments, we can still expect to draw some sensible conclusions about the mechanisms that are relevant to this problem, and note that shallow water and thin film models,

TABLE I. Typical values for the parameters taken from Ref. [1].

Parameter	Symbol	Typical Value	Units
Volume	V_o	5×10^{-9}	m^3
Contact angle	θ_0	1.08	rad
Density	ρ	1190	$\mathrm{kg\,m^{-3}}$
Viscosity	ν	3.1×10^{-5}	$\mathrm{m^2\,s^{-1}}$
Surface tension	σ	0.066	$\mathrm{kg\,s^{-2}}$
Acceleration	a_0	174	$\mathrm{m\,s^{-2}}$
Frequency	f	50.77	$\mathrm{s^{-1}}$
Slope	α	$\pi/4$	rad

which are also based on a small slope approximation, often produce reasonable results, even when this assumption is not strictly satisfied in the underlying physical problem. Two other important dimensionless parameters are

$$\delta_1 \approx 0.13, \quad \delta_2 \approx 0.042,$$

which shows that inertia is more important than viscous forces, and that we can reasonably neglect them both at leading order compared to surface tension and the applied acceleration. Finally,

$$\epsilon \approx 1.63, \quad \gamma \approx 1.08, \quad \omega \approx 3.06, \quad \bar{a} \approx 0.056,$$

which shows that the small ϵ asymptotic solution is not likely to be a good approximation for the actual experiment. A similar comparison is carried out in Sec. V of Ref. [15], which agrees that the quasistatic approximation will hold for some of the experiments. Now that we have covered how physically realistic our model is, the next step is to apply the assumptions we are using and obtain the governing equations. If we nondimensionalize Eq. (1) and keep only the leading order terms for $\delta_1, \delta_2 \ll 1$ (neglecting both the inertial term and viscous term, respectively) we are left with

$$p(\mathbf{x},t) = -\epsilon a(t)(x + \gamma z) - F(t), \tag{8}$$

where the gradient operator has been integrated out producing an arbitrary function, $F(t)$. The dimensionless effective gravity is now given by $a(t) = \bar{a} + \sin(\omega t)$ with $\bar{a} = g/a_0$. Now if we also nondimensionalize Eq. (3) and keep only the leading order terms for $\theta_0 \ll 1$ we are left with

$$p = -\tilde{\nabla}^2 h, \quad \text{on } z = h(x,y,t), \tag{9}$$

where $\tilde{\nabla}^2 = \frac{\partial^2}{\partial x^2} + \frac{\partial^2}{\partial y^2}$. By combining Eqs. (8) and (9) on the free surface, $z = h(x,y,t)$, we can reduce this three-dimensional problem to a two-dimensional one where the height of the droplet is an unknown variable. The new equation (with ˜ above the ∇ omitted) is

$$[\nabla^2 - \epsilon\gamma a(t)]h(x,y,t) = \epsilon a(t)x + F(t), \tag{10}$$

while the boundary condition for the height of the droplet along the contact line remains

$$h(\mathbf{x},t) = 0 \quad \text{for } x,y \in \partial\mathcal{R}(t). \tag{11}$$

Equation (5) becomes

$$\iint_{\mathcal{R}(t)} h(x,y,t)\,dx\,dy = 2\pi, \tag{12}$$

and Eq. (6) becomes

$$\mathbf{n} \cdot \frac{\partial \mathbf{X}}{\partial t} = \theta - 1 + \frac{1}{2}v''(\theta - 1)^2 + O(\theta - 1)^3, \tag{13}$$

where $U = V'\theta, v'' = V''\theta_0^2/U$ and $\mathbf{X} = (x,y) \in \partial\mathcal{R}(t)$. We will modify Eq. (13) in later sections so that we can study different contact line laws, including hysteresis. Note that $a(t)$ changes sign as a function of time, so that the homogeneous form of Eq. (10) is either Helmholtz equation, a modified Helmholtz equation, or Laplace's equation as t varies.

In order to solve Eqs. (10)–(13) we first redefine the height, $h(x,y,t)$, in order to absorb the right-hand side of Eq. (10) leaving the remaining equation homogeneous. The redefined height is then a known function on the boundary, and we can use a boundary integral formulation [16] to find the normal derivative of the height on the boundary (i.e., the contact angle) for a given contact line, $\partial\mathcal{R}(t)$. Note that, depending on whether a is greater than, less than, or equal to zero, the Green's function is either a modified Bessel function, a Bessel function, or a logarithm, respectively. We use this boundary integral approach to evolve the boundary (i.e., the contact line), which we discretize using linear elements, with Crank-Nicolson time stepping. This method is second-order accurate in both space and time, confirmed by standard convergence tests.

III. RESULTS

A. Comparison of numerical and asymptotic solutions

We will begin by comparing our numerical solution of Eqs. (10)–(13) to Benilov's asymptotic solution for $\epsilon \ll 1$ [11]. The main results that Benilov obtained was the rise velocity of the droplet,

$$V_r^{(B)} = \epsilon^2\left[\frac{\gamma[3 + 4\omega^2(1 - v'')]}{12(9 + 4\omega^2)} - \frac{\bar{a}}{\epsilon}\right]. \tag{14}$$

We can deduce from this that $V_r^{(B)}$ is monotone increasing with ω for $v'' < 2/3$, monotone decreasing for $v'' > 2/3$, and independent of ω for $v'' = 2/3$. Although Benilov included the quadratic term in the Taylor expansion of the contact line law in Ref. [11], for larger values of ϵ, for which the range of contact angles that are driven by the oscillation, is larger, this leads to an unphysical model, since the contact line velocity may be a decreasing function of contact angle. We therefore focus on the case $v = 0$ for our fully nonlinear simulations, as well as an alternative, cubic law, in Sec. III C. We also know that when $\bar{a} = O(\epsilon)$, $V_r^{(B)}$ is proportional to ϵ^2. Rearranging Eq. (14) also gives us the condition for zero rise velocity,

$$\epsilon = \bar{a}\frac{12(9 + 4\omega^2)}{\gamma[3 + 4(1 - v'')\omega^2]}. \tag{15}$$

These are the two results with which we will compare our solutions. We first fix ϵ and γ and examine the rise velocity, V_r and $V_r^{(B)}$, as ω varies. Figure 2 shows a comparison between our results and the asymptotic solution for a linear contact line law and a quadratic one with $v'' = 0.4$, which shows good accuracy for small ϵ. The other comparison, a curve showing zero rise velocity, is the left graph given in Fig. 7, which is discussed in the next section. Our next goal will be to include contact angle hysteresis in the model and to examine how and why this affects the rise velocity. Before we do this we take Eqs. (33) and (35) from Ref. [11] and write the first-order correction for the radius of the droplet as a function of polar angle ϕ, in a stationary frame of reference as

$$R^{(1)}(\phi,t) = \epsilon\left[\frac{\gamma}{12}\frac{3\sin\omega t - 2\omega\cos\omega t}{9 + 4\omega^2} + \frac{1}{\omega}\cos\omega t\cos\phi\right],$$

where $\phi = 0$ is the positive x axis. This is the leading-order motion of the droplet and it consists of a term with ϕ dependance—the swaying mode—and a term without—the spreading mode. Although these two modes are independent of each other at leading order and individually give no net motion, the nonlinear interaction between the two causes the

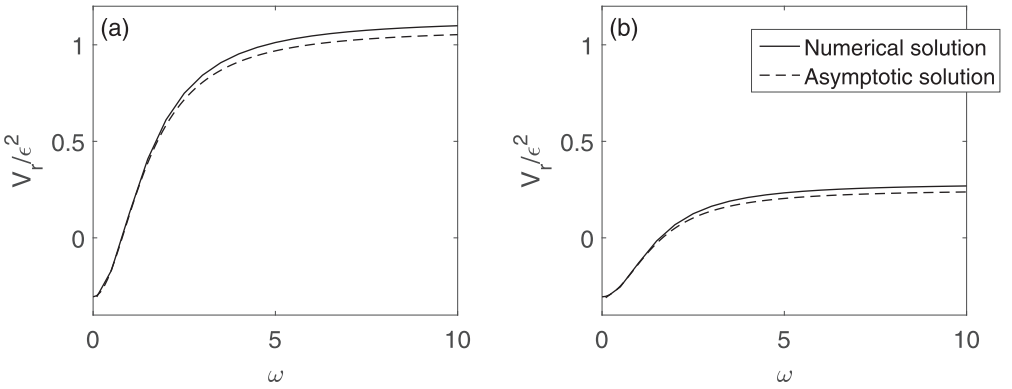

FIG. 2. Comparison between numerical and asymptotic solutions for the rise velocity of a droplet on an inclined plane against the frequency with $\epsilon = 0.04, \gamma = 25$, and $v'' = 0$ (a), 0.4 (b).

droplet to climb or slide, [11,12]. If we write this in terms of a phase shift we obtain

$$R^{(1)}(\phi,t) = \epsilon\left\{\frac{\gamma}{3}\frac{\cos[\omega t - \tan^{-1}(2\omega/3) - \pi/2]}{\sqrt{9+4\omega^2}} + \frac{\cos\omega t}{\omega}\cos\phi\right\}, \tag{16}$$

and we can see that the phase difference between the two modes varies monotonically with ω from $\pi/2$ out of phase when $\omega = 0$ to fully in phase as $\omega \to \infty$. What we can conclude from Ref. [11] is that for a linear contact line law ($v'' = 0$) the largest rise velocity occurs when the spreading and swaying modes are in phase, in qualitative agreement with Ref. [12]. We will use this result to help understand how the addition of contact angle hysteresis to the model changes the rise velocity.

B. The effect of hysteresis

Now that we have some confidence in our numerical solution method, we include contact angle hysteresis in the model, so that $\theta_A > \theta_R$. When ϵ is sufficiently small, this pins the whole contact line, so that the droplet cannot move. We will begin by considering the case $\epsilon = 0.04$, $\gamma = 25$, and $v'' = 0$, which we studied in the previous section. With the inclusion of hysteresis in the problem we can no longer define θ_0 as the angle at which the contact line is stationary and so we redefine it as

$$\theta_0 = \frac{h_0}{R_0}, \tag{17}$$

where h_0 is the height of the unperturbed droplet. We scale both θ_A and θ_R using this redefined θ_0. The hysteresis interval is defined to be the difference between these scaled advancing and receding angles. Figure 3 shows the rise velocity of the droplet for increasing hysteresis intervals with $\epsilon = 0.04$, $\gamma = 5$ and a linear contact line law. A small hysteresis interval has little effect on the overall motion of the droplet. However, with a large enough hysteresis interval, for $\omega = O(1)$, the droplet climbs uphill instead of sliding down and the rise velocity is not as large for sufficiently large values of ω. We can also see that for sufficiently large hysteresis intervals the droplet oscillates, but the contact line is fully pinned.

We have seen how the leading order motion of a droplet on an inclined plane with small amplitude oscillations can be written as a combination of two independent modes; spreading and swaying. We can also see from Eq. (16) that the spreading mode scales linearly with γ and so we will examine how the size of this parameter affects the interaction between the modes under the influence of contact angle hysteresis. Since ϵ is not necessarily small, we extract the nonlinear spreading mode by plotting the rate of change of distance between the leading and trailing edges of the droplet on the line of symmetry, and the nonlinear swaying mode by plotting the velocity of the midpoint of these edges (the center of the droplet).

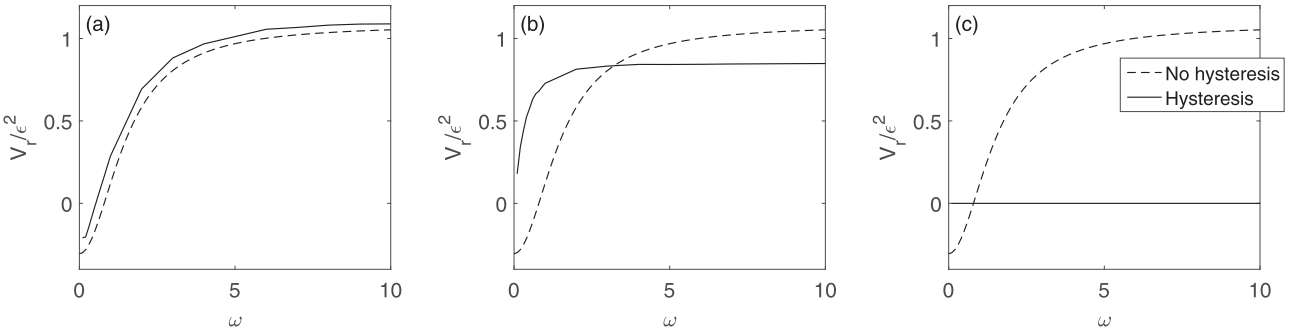

FIG. 3. Rise velocity of a droplet against the frequency where $\epsilon = 0.04$, $\gamma = 25$, a linear contact line law and a hysteresis interval of 0.02 (a), 0.2 (b), 0.4 (c). The dashed line represents the rise velocity of the droplet for the same parameter values but no contact angle hysteresis present.

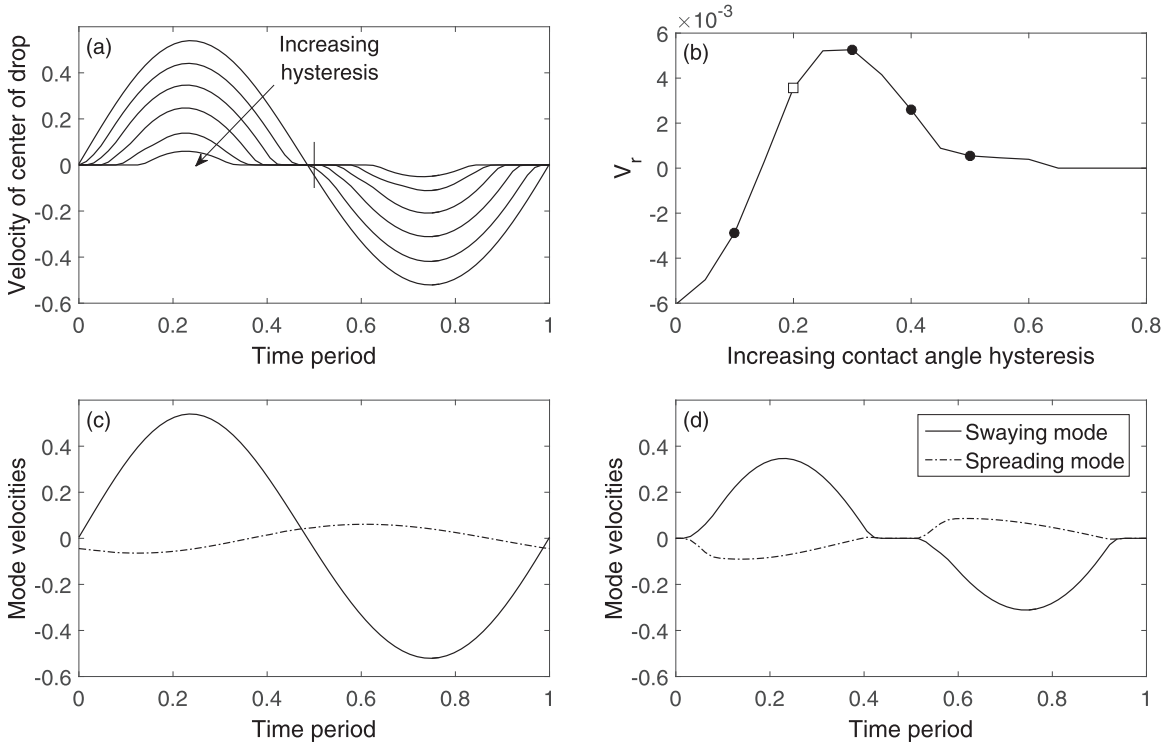

FIG. 4. (a) The velocity of the center of the droplet (taken along the x axis) over one period of oscillation for increasing contact angle hysteresis. (b) The rise velocity of the droplet for increasing contact angle hysteresis. (c, d) The velocity of of the swaying and spreading modes over one period of oscillation for no hysteresis and a hysteresis interval of 0.2, respectively. Each of the markers on (b) coincide with the velocity profiles on (a) with the white squares also matching the results shown in (c) and (d). The parameters are $\epsilon = 0.53$, $\gamma = 1$, $\omega = 1.5$, $\bar{a} = 1/25$, and $v'' = 0$.

When $\gamma = 1$, the amplitude of the spreading mode is smaller than that of the swaying mode so we will focus on the latter. We can see in Fig. 4(a) that increasing the size of the hysteresis interval reduces the magnitude of the velocity of the center of the droplet. In the absence of hysteresis, the droplet spends more time sliding than it does climbing, and the magnitude of the peak is slightly larger than that of the trough [these features can be seen more clearly in Fig. 5(a)]. The area under the climbing section of the graph is smaller than that under the sliding section, so the net motion of the droplet is down the substrate. When there is a nonzero hysteresis interval, both the peak and the trough are reduced, and more sliding is removed from the motion than climbing, so that, for a large enough hysteresis interval, the net motion of the droplet is climbing [Fig. 4(b)]. This continues up to a peak rise velocity at a critical hysteresis interval such that for larger intervals the droplet rise velocity decreases and becomes pinned for sufficiently large hysteresis.

When $\gamma = 25$, the amplitude of the spreading mode is comparable to that of the swaying mode [Fig. 5(c)], and there is a phase difference between them that is controlled by ω. When $\omega = 1.5$ as shown in Fig. 5, the phase difference is about $\pi/4$ and, in the absence of hysteresis, the droplet slides down the substrate. However, when hysteresis is included, the amplitudes of spreading and swaying modes are forced to be zero at the same time, i.e., the leading and trailing contact lines are both pinned [Fig. 5(d)]. This forces the two modes into phase, and the droplet climbs. As before, for large enough hysteresis intervals, the droplet becomes pinned. When $\omega = 20$, shown in Fig. 6, the modes are approximately in phase in the absence of hysteresis. Because of this, the inclusion of hysteresis does not cause a dramatic increase in the rise velocity as it did in the previous two cases. The rise velocity generally decreases as the hysteresis interval increases, but not monotonically, and in a manner that reflects the strong nonlinearity of the system. This example helps to explain why the rise velocity of the droplet is smaller for large enough ω in Fig. 3.

We conclude this section by considering how the sliding-climbing phase diagram as a function of frequency and amplitude is affected by hysteresis, as shown in Fig. 7. In the absence of hysteresis, the phase diagram is very similar to Fig. 4 in Ref. [11] (with differences coming from the fact that ϵ ranges from 0.56to1.24). When hysteresis is included a smaller value of ϵ is required to make the droplet climb and also a static region (where the droplet is pinned) appears for very small ϵ. There is no pinned region between the sliding and climbing sections on the hysteresis phase diagram, unlike the experimental phase diagram that appears in Ref. [1], which indicates that is an effect of some of the physics neglected in our simple model.

C. Alternative contact line law

So far we have considered the contact line law to be a linear function of the contact angle. However, other models have been considered in the literature, one of which we study here to see how much it affects the motion of the droplet. Specifically, we

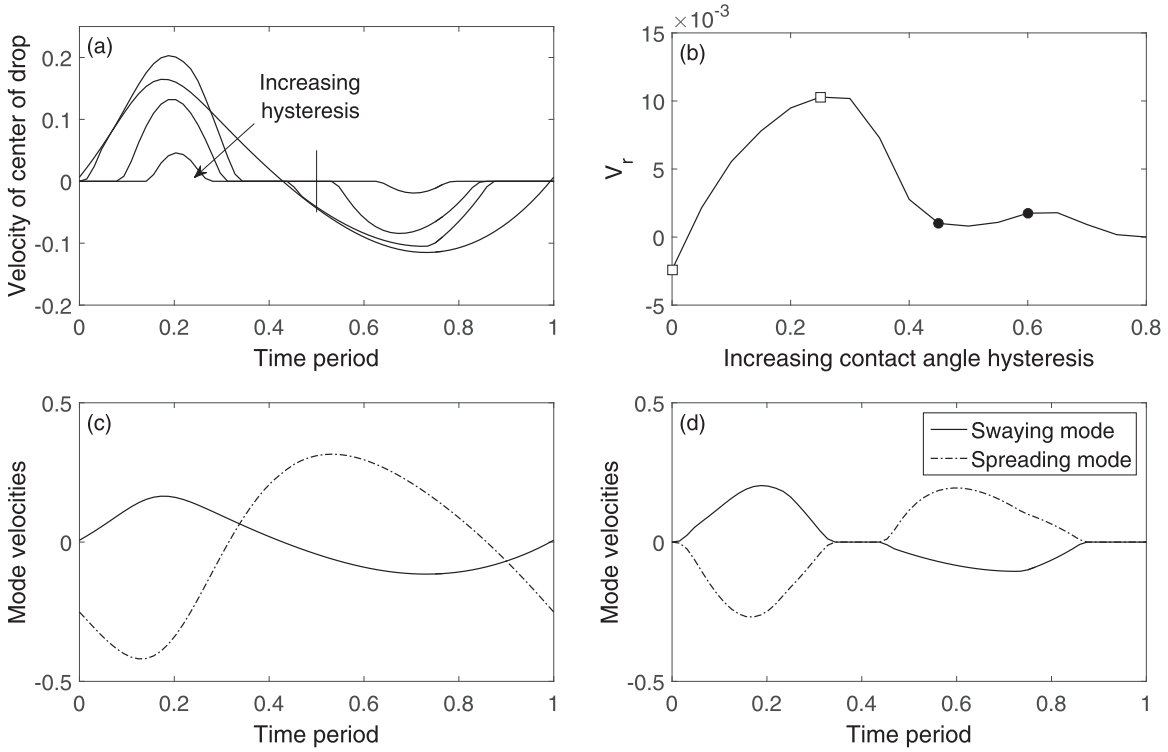

FIG. 5. (a) The velocity of the center of the droplet (taken along the x axis) over one period of oscillation for increasing contact angle hysteresis. (b) The rise velocity of the droplet for increasing contact angle hysteresis. (c, d) The velocity of of the swaying and spreading modes over one period of oscillation for no hysteresis and a hysteresis interval of 0.2, respectively. Each of the markers on (b) coincide with the velocity profiles on (a) with the white squares also matching the results shown in (c) and (d). The parameters are $\epsilon = 0.125$, $\gamma = 25$, $\omega = 1.5$, $\bar{a} = 1/5$, and $v'' = 0$.

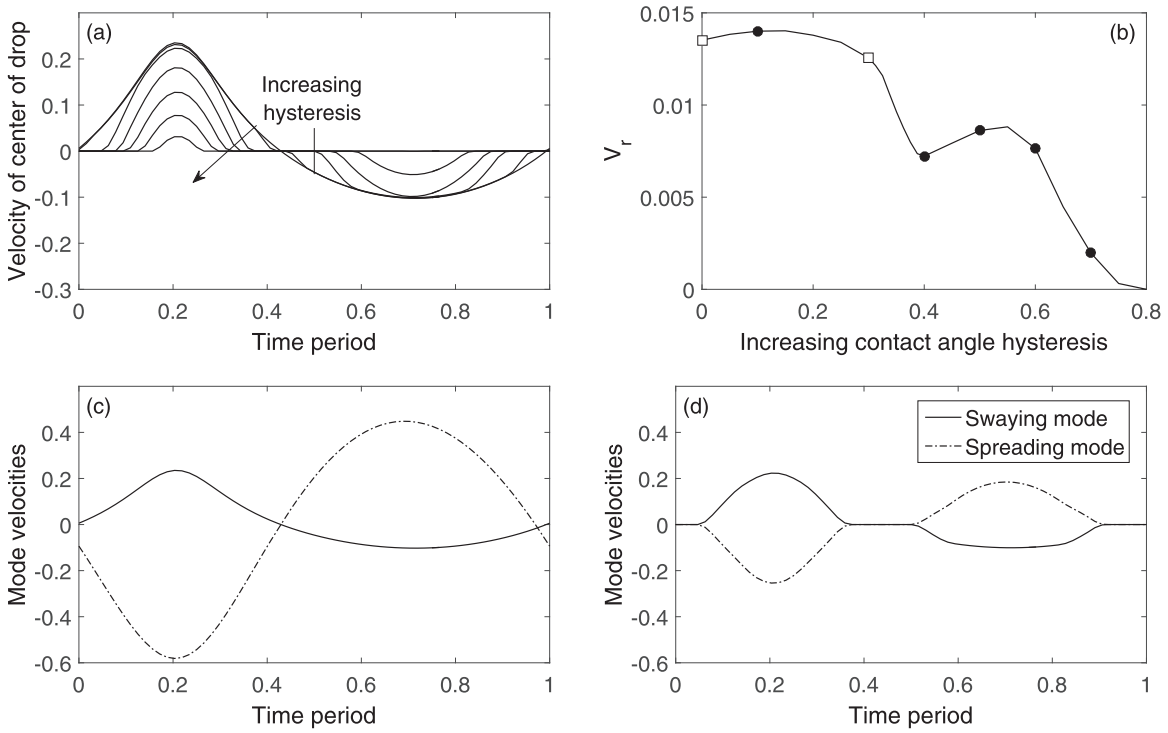

FIG. 6. (a) The velocity of the center of the droplet (taken along the x axis) over one period of oscillation for increasing contact angle hysteresis. (b) The rise velocity of the droplet for increasing contact angle hysteresis. (c, d) The velocity of of the swaying and spreading modes over one period of oscillation for no hysteresis and a hysteresis interval of 0.2, respectively. Each of the markers on (b) coincide with the velocity profiles on (a) with the white squares also matching the results shown in (c) and (d). The parameters are $\epsilon = 0.125$, $\gamma = 25$, $\omega = 20$, $\bar{a} = 1/5$, and $v'' = 0$.

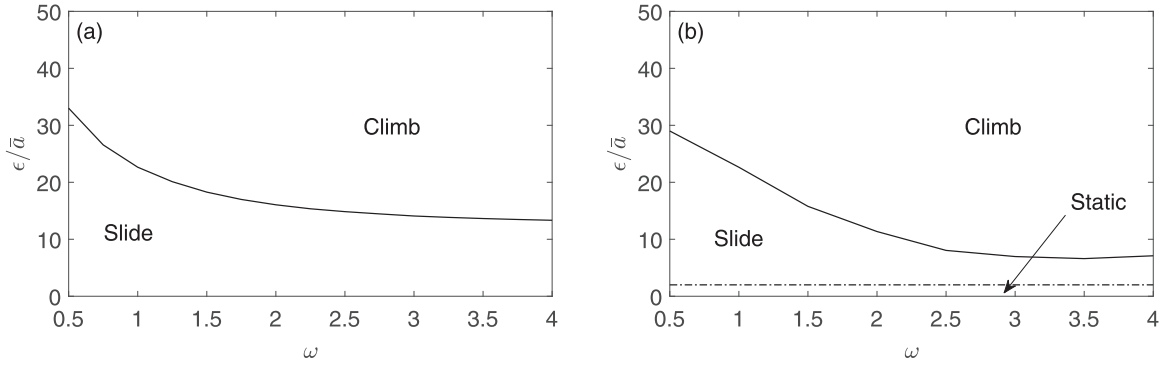

FIG. 7. A slide-climb phase diagram for the droplet with no hysteresis (a), a hysteresis interval of 0.2 (b) for $\gamma = 1$ and a linear contact line law.

consider the cubic contact line law given by

$$\hat{v}(\hat{\theta}) = \begin{cases} v_A|\hat{\theta} - \hat{\theta}_A|^3 & \text{for } \hat{\theta} \geqslant \hat{\theta}_A, \\ 0 & \text{for } \hat{\theta}_A > \hat{\theta} > \hat{\theta}_R, \\ -v_R|\hat{\theta} - \hat{\theta}_R|^3 & \text{for } \hat{\theta}_R \geqslant \hat{\theta}, \end{cases} \tag{18}$$

in dimensionless form where $v_{A,R}$ are dimensionless velocities. In the absence of hysteresis, this has been shown to agree with experimental results for slow, steady flows [5]. For simplicity we will take $v_{A,R} = 1$.

For small ϵ, we would expect the variation in the contact angle to scale with ϵ, so the cubic law leads to smaller contact line velocities than the linear law for small forcing. In addition, the nonlinearity of the cubic contact line law leads to the spreading and swaying modes being in phase for small ω and the inclusion of hysteresis leads to a smaller rise velocity, in contrast to the results for a linear contact line law. The latter can be seen more clearly in Fig. 8, which has parameter values identical to the results shown in Fig. 5 for the linear contact line law. When there is no hysteresis the shape of the swaying mode is very similar for linear and cubic laws, with obvious differences at small contact line velocities. However, for the cubic law, when hysteresis is included, the rise velocity of the droplet decreases as a function of hysteresis interval, since the modes are already in phase, and the velocity profile changes in a manner similar to that shown in Fig. 4 for the linear law. This is consistent with our explanation that the increase in

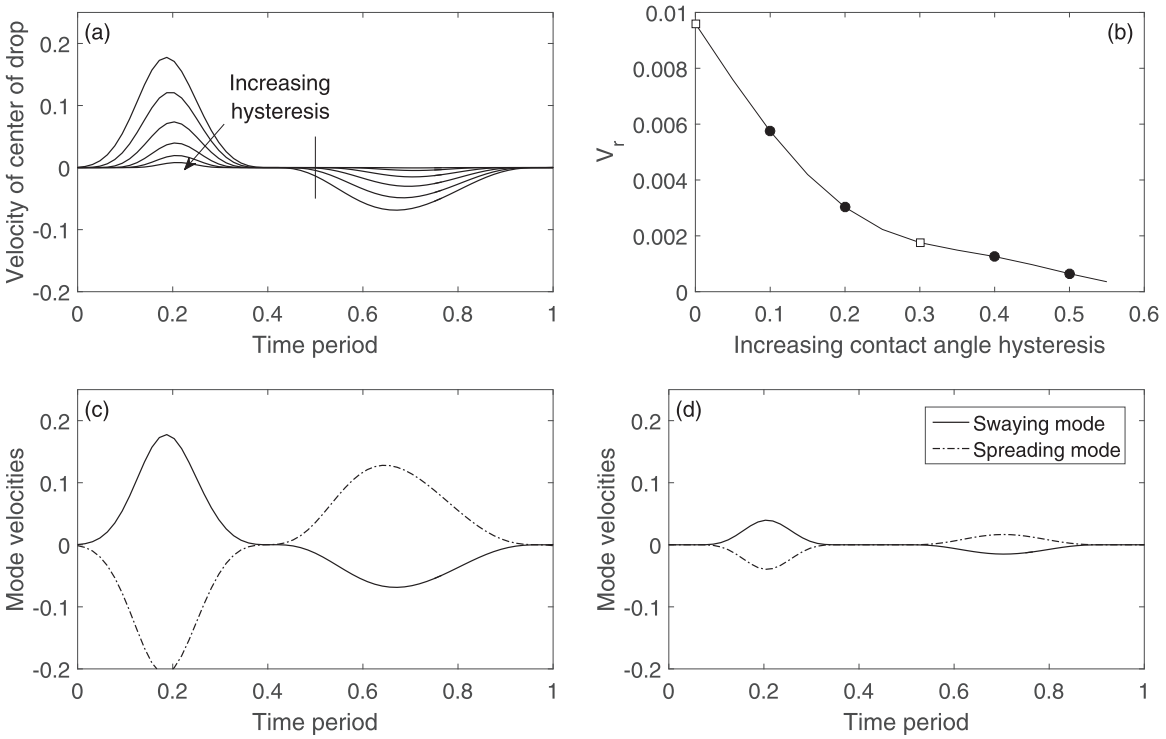

FIG. 8. (a) The velocity of the center of the droplet (taken along the x axis) over one period of oscillation for increasing contact angle hysteresis. (b) The rise velocity of the droplet for increasing contact angle hysteresis. (c, d) The velocity of of the swaying and spreading modes over one period of oscillation for no hysteresis and a hysteresis interval of 0.2, respectively. Each of the markers on (b) coincide with the velocity profiles on (a) with the white squares also matching the results shown in (c) and (d). The parameters are $\epsilon = 0.125$, $\gamma = 25$, $\omega = 1.5$, $\bar{a} = 1/5$, and a cubic contact line law.

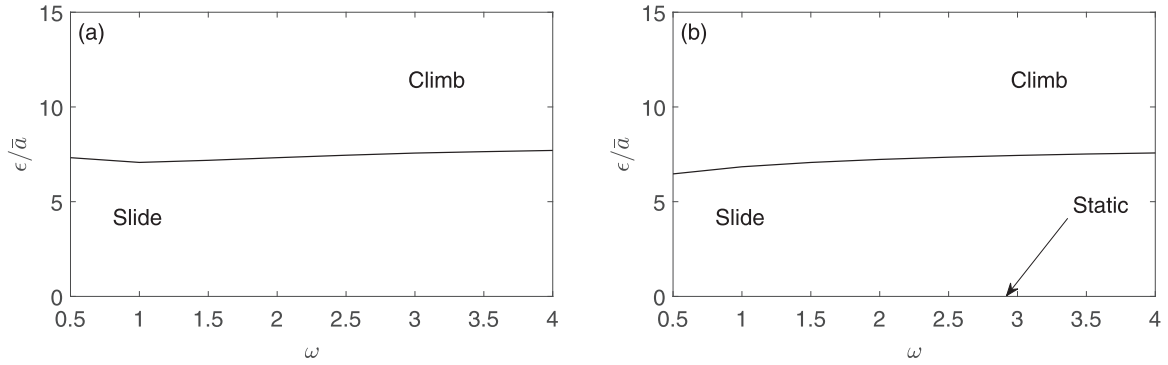

FIG. 9. A slide-climb phase diagram for the droplet with no hysteresis (a) and a hysteresis interval of 0.2 (b) for $\gamma = 1$ and a cubic contact line law.

rise velocity is due to the phase difference of the modes being forced to zero.

Finally, consider the phase diagrams shown in Fig. 9. In contrast to the phase diagrams for a linear contact line law, shown in Fig. 7, hysteresis has little effect on the slide-climb boundary because the swaying and spreading modes are in phase when there is no hysteresis. In addition, the position of the boundary is only a very weak function of ω as it has little effect on the phase difference between the modes. Note that a similar phase diagram can occur for the original contact line law, Eq. (15), with $v'' = 2/3$.

D. Droplet footprints

Finally, we will briefly study how the shape of the footprint of the droplet changes as it moves across the substrate. We will look at how it differs with or without hysteresis and also how changing the contact line law affects it. As well as looking at how the droplet evolves as the substrate oscillates we can first examine the footprint for the simplified case of a stationary substrate, where the droplet slides down the plane. If there is no hysteresis, or if $(\theta_A + \theta_R)/2 = 1$, so that the hysteresis interval is symmetric, the footprint remains close to circular as it slides. The shape is more interesting for an asymmetric hysteresis interval and a small receding contact angle. In this case, the droplet deforms in three stages (shown in Fig. 10). The first stage of the motion is for the lower half to slide down the plane with the top half moving more slowly. The lower half also thins in the lateral direction, whereas the upper half spreads out slightly. We will see similar behavior when the plane is oscillating (Fig. 11). However, unlike the unsteady flow, the droplet continues to move in the same direction and in the second stage of the initial motion the receding contact line begins to catch up with the advancing contact line. The lower part of the droplet is noticeably narrower than the upper part. As the droplet continues to slide, the top of the droplet also thins laterally, until a steady state is reached in which the lateral thickness of the droplet has reached an equilibrium value somewhat smaller than the initial width. It has been shown [17] that, for a model with prescribed values for the advancing and receding contact angles, the final shape given in Fig. 10 is in fact the only shape that has no singularities.

When the plate is oscillating, for a linear contact line law with no hysteresis, or if the hysteresis interval is symmetric, as for the steady flow, the footprint remains circular. For asymmetric hysteresis intervals, the footprint is almost circular with the base of the droplet expanding slightly for $(\theta_A + \theta_R)/2 < 1$ or contracting slightly for $(\theta_A + \theta_R)/2 > 1$. Although these are not significant, changing the contact line law can make a big difference.

Figure 11 shows what the footprint looks like for a cubic contact line law with $\theta_R = 0.5$ and $\theta_A = 1.1$. The droplet slides and the lower part of the contact line moves a lot

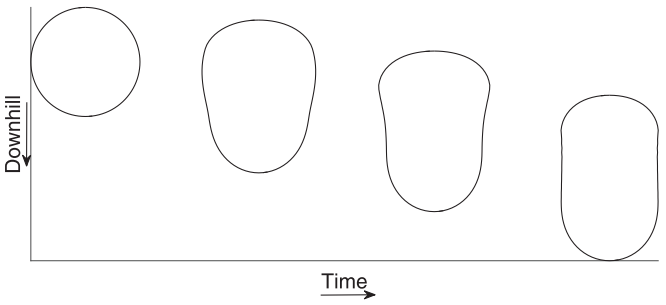

FIG. 10. The four stages a sliding droplet undergoes on a stationary substrate ranging from an unperturbed shape to its steady state (from left to right, respectively) for $\epsilon = 0.4$, $\gamma = 5$, $\omega = 0$, a linear contact line law, $\theta_A = 1.1$ and $\theta_R = 0.4$. Constant time increments have been taken in between each stage.

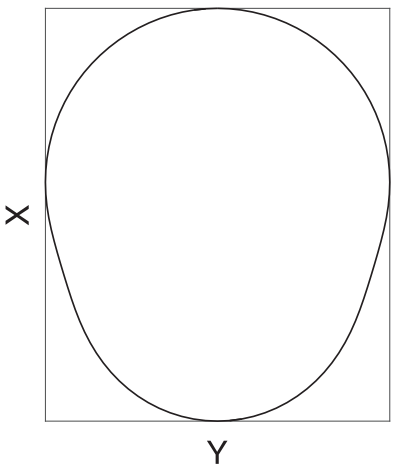

FIG. 11. Example footprint of a sliding droplet, for $\epsilon = 0.44$, $\gamma = 4.5$, $\omega = 5$, a cubic contact line law, $\theta_A = 1.1$ and $\theta_R = 0.5$.

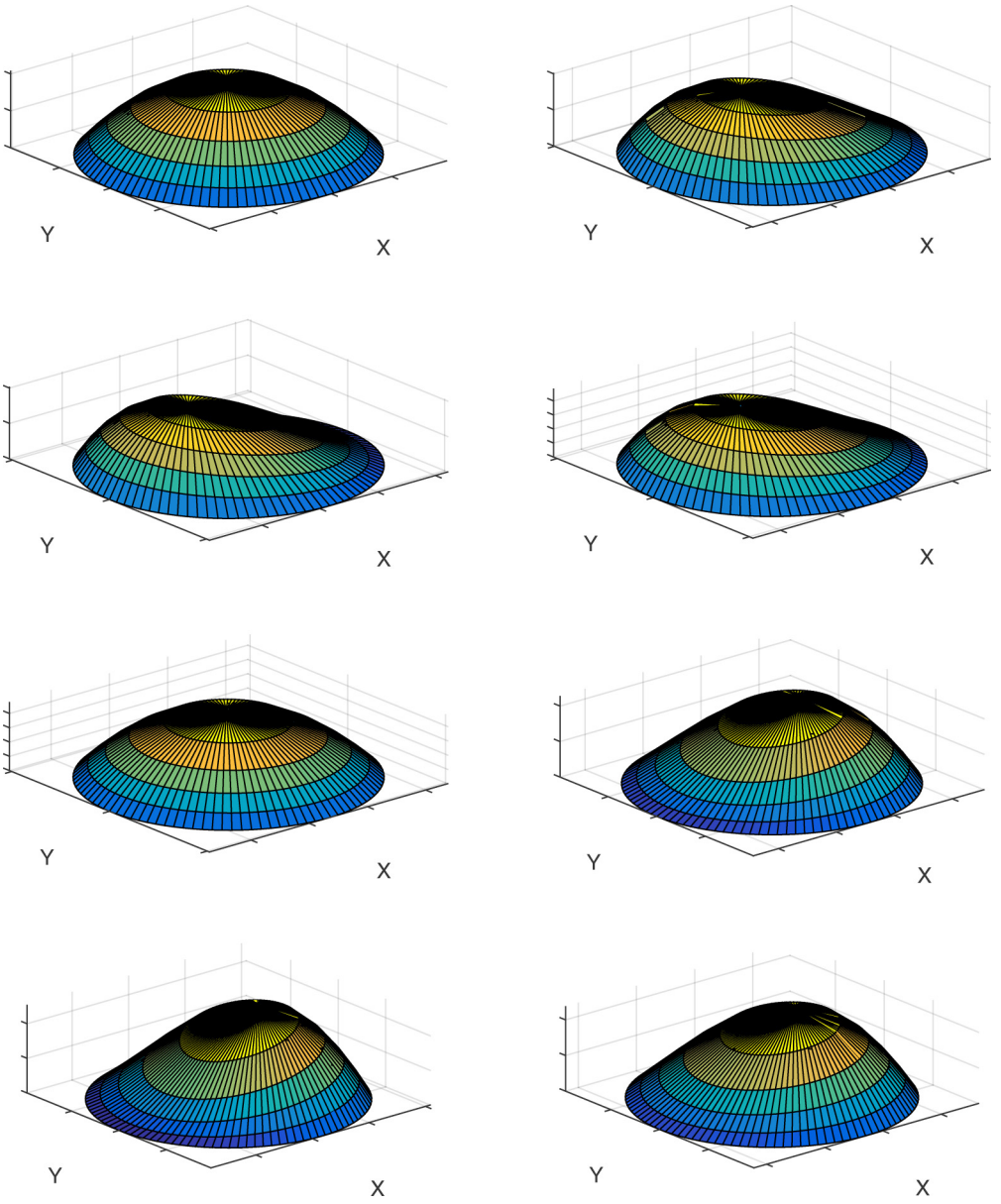

FIG. 12. 3D plots of the motion undergone by a droplet over the course of one time period for $\epsilon = 0.8$, $\gamma = 1$, $\omega = 1$, a linear contact line law, $\theta_A = 1.1$ and $\theta_R = 0.9$. Constant time increments have been taken in between each stage.

more than the upper part. The droplet deforms mainly in the downhill direction. This is the most interesting footprint shape, as it resembles results shown in Fig. 4 of Ref. [1] very closely. The final result we will show is a three-dimensional plot of a droplet as it oscillates over one time period (Fig. 12).

IV. CONCLUSIONS

In this paper we considered the motion of surface tension dominated, oscillating droplets, and neglected the effects of inertia and viscosity. We also assumed that the slope of the free surface is small. If the amplitude of the oscillation is sufficiently small we found that the motion of the droplet can be separated into two modes and the nonlinear interaction between them causes the droplet to slide or climb. The droplet can climb uphill for most parameter values as long as the frequency of the oscillation is large enough with the rise velocity reaching its maximum when the two modes are in phase. Adding hysteresis can cause an otherwise sliding droplet to climb by forcing the two modes into phase producing a larger rise velocity. Although we could not compare this model directly to the experimental results in Ref. [1] it is possible to obtain footprints similar to those observed in the actual experiment. We also looked at how a small receding contact angle leads to noncircular contact lines. In spite of the strong simplifications that we used, we have been able to examine the effect of contact angle hysteresis on the rise or fall of strongly driven droplets.

ACKNOWLEDGMENT

The authors acknowledge the support of the EPSRC DTG under Grant No. RS2238.

[1] P. Brunet, J. Eggers, and R. D. Deegan, Phys. Rev. Lett. **99**, 144501 (2007).
[2] X. Noblin, R. Kofman, and F. Celestini, Phys. Rev. Lett. **102**, 194504 (2009).
[3] E. B. Dussan V. and S. H. Davis, J. Fluid Mech. **65**, 71 (1974).
[4] L. Hocking, J. Fluid Mech. **76**, 801 (1975).
[5] L. Tanner, J. Phys. D: Appl. Phys. **12**, 1473 (1979).
[6] L. Hocking, Phys. Fluids **6**, 3224 (1994).
[7] N. Savva and S. Kalliadasis, J. Fluid Mech. **725**, 462 (2013).
[8] J. Billingham, J. Fluid Mech. **464**, 365 (2002).
[9] D. Lyubimov, T. Lyubimova, and S. Shklyaev, Phys. Fluids **18**, 012101 (2006).
[10] C.-L. Ting and M. Perlin, J. Fluid Mech. **295**, 263 (1995).
[11] E. S. Benilov, Phys. Rev. E **84**, 066301 (2011).
[12] E. Benilov and J. Billingham, J. Fluid Mech. **674**, 93 (2011).
[13] K. John and U. Thiele, Phys. Rev. Lett. **104**, 107801 (2010).
[14] J. Sullivan, S. Wilson, and B. Duffy, Q. J. Mech. Appl. Math. **61**, 25 (2008).
[15] E. S. Benilov and C. P. Cummins, Phys. Rev. E **88**, 023013 (2013).
[16] C. Pozrikidis, *A Practical Guide to Boundary Element Methods with the Software Library BEMLIB* (Chapman and Hall, London, 2002).
[17] E. B. Dussan V. and R. T.-P. Chow, J. Fluid Mech. **137**, 1 (1983).